2021-01-20

Synthesis of Ultrafine Co 1(x+y) Ni x Zn y Fe 2 O 4 Ferrite Nanoparticles: Customizing Magnetic Properties

Khorshidian, S

10.1002/slct.202004461
ChemistrySelect
Wiley

Materials Science inc. Nanomaterials & Polymers

Synthesis of Ultra-fine $Co_{1-(x+y)}Ni_xZn_yFe_2O_4$ Ferrite Nanoparticles: Customizing Magnetic Properties

Sara Khorshidian,[a] Behrooz Vaseghi,*[a] Ghasem Rezaei,*[a] David Jenkins,[b] Niroj Kumar,[c] and Arunima Rajan[c, d]

Synthesis of ultrafine $Co_{1-(x+y)}Ni_xZn_yFe_2O_4$ magnetic nanoparticles with different chemical compositions is essential to study the magnetic fluid hyperthermia (MFH) as a treatment in which the superparamagnetic behaviour of materials is beneficial. In this paper, $Co_{1-(x+y)}Ni_xZn_yFe_2O_4$ magnetic nanoparticles with different x and y amounts were synthesized to find out a tuning pattern for magnetic properties, especially anisotropy constant to gain the best heating efficiency. We proved that the co-presence of ions will greatly affect the magnetic performance of our superparamagnetic nanoparticles in which $Co_{0.59}Zn_{0.41}Fe_2O_4$ for values of $x = 0.00$ and $y = 0.41$ exhibits the highest magnetic anisotropy constant after $CoFe_2O_4$ $CoFe_2O_4$. This success in customizing magnetic properties to reach high magnetic properties by using less toxic materials might be another good starting point for researchers to focus more on their possible applications.

Introduction

Due to their peculiar magnetic properties and small dimensions, magnetic nanoparticles (MNPs) have a wide variety of properties and hence applications in different areas of science and technology, including electromagnetic sensors and devices[1,2], MRI imaging[3], design and fabrication of biomedical devices[3], hyperthermia increasing temperature of cancerous tissue[4,5], drug delivery and other biomedical applications[6–9], electrochemical sensors[10], supercapacitor applications[10], water purification[11] and so on. Being more precise, in biomedical applications, by approaching the nanosize scale, one can get close to biological entities of interest. Indeed, coating nanoparticles with biological molecules for interacting with or binding to a biological entity provides a controllable means of 'tagging' or addressing it. On the other hand, their magnetic properties lead to manipulate them by an external magnetic field gradient[8,12,13].

Depending on the particle size, the injected material may exhibit a multi-domain, single-domain or superparamagnetic (SPM) M–H curve. In superparamagnetic nanoparticles the energy delivered to the particle is needed to coherently align the particle moments to approach the saturated magnetization state[12,14,15]. It is known that healthy cells can tolerate temperatures even higher than $42^{\circ}C$ while cancer cells are much more sensitive to temperature, hence by increasing the environment temperature above the threshold to the temperatures between $41^{\circ}C$and $46^{\circ}C$ for at least 30 minutes, cancer cells will be destroyed[12,16,17]. Magnetic hyperthermia treatment is a procedure which uses this fact as a treatment for cancer by using magnetic nanoparticles. Magnetic fluid hyperthermia (MFH) is a hyperthermia treatment in which you can get the advantage of superparamagnetic materials with almost zero coercive fields as a suspended nanoparticle in water or hydrocarbon fluid which is called ferrofluid. So, if there exists a safe process to disperse magnetic nanoparticles in the infected area (tumors), then by applying an AC magnetic field of sufficient strength and frequency in the radio frequency spectrum with allowable upper limit of $2.5 \times 10^6\ Oe.s^{-1}$, the cancer cell can be treated and destroyed[14,16–22]. The heat generation from magnetic particles under applied magnetic field is usually quoted in terms of the specific absorption rate (SAR) in units of $W.g^{-1}$[20]. Elvira Fantechi et al in 2015 published their report on the influence of cobalt doping on the hyperthermic efficiency of magnetite nanoparticles. They also concluded that the higher magnetic anisotropy provides better heating efficiency[23]. As in any application, using less toxic material is important to reduce any harmful side effect of the final product. Cobalt ferrites have wide applications, but if it is possible to produce the same properties with a less toxic component, it has made a big step toward bio applications. With heavy metal ions (here; Co, Ni, and Zn), Zn has the less toxicity[24,25].

The magnetic properties essential for biomedical applications, such as saturation magnetization, coercivity and magnetocrystalline anisotropy is primarily governed by the lattice structure of the material. The cation distribution and composition in their crystal structure is an effective parameter for

[a] S. Khorshidian, Dr. B. Vaseghi, Dr. G. Rezaei
Department of Physics, College of Sciences, Yasouj University, Yasouj, 75918-74934, Iran
E-mail: vaseghi@yu.ac.ir
grezaei@yu.ac.ir
[b] Dr. D. Jenkins
Wolfson Nanomaterials & Devices Laboratory, School of Computing, Electronics and Mathematics, Plymouth University, Devon, PL4 8AA, UK
[c] Dr. N. Kumar, A. Rajan
Centre for Nanotechnology Research, Vellore Institute of Technology, Vellore, 632014, India
[d] A. Rajan
School of Advanced Sciences, Vellore Institute of Technology, Vellore, 632014, India

Supporting information for this article is available on the WWW under https://doi.org/10.1002/slct.202004461

changing the properties of ferrite MNPs. Substitution of ions in the lattice structure has always been a challenging issue for the researches to gain desired properties[26,27]. Arulmurugan et al. have investigated the substitution of Co ions by Zn ions to decrease the saturation magnetization and particle size of their MNPs[28–30]. In another report by Tumar and coworkers, the structure of

$Co_{0.5}Zn_{0.5}Fe_2O_4$has been investigated as a particle with ferrimagnetic and superparamagnetic behavior[31]. There are many studies on the superposition of cations which include a wide variety of compositions from simple ferrites to the more complex ones such as $Mg_{0.3+x}Cu_{0.2}Zn_{0.5-x}Fe_{1.98}O_4$ that has been reported by Wang et al at.[32]. To name, Sathishkumar et al. are another group who investigated the substitution of Ni^{+2} ion as in a three-component $Co_{0.5-x}Ni_xZn_{0.5}Fe_2O_4$ ferrite with constant Zn value in the composition[33].

In spinel ferrites the metal ions are situated in two different sublattices designated tetrahedral and octahedral according to the geometrical configuration of the oxygen nearest neighbors. There are 64 tetrahedral (A-site) and 32 octahedral interstitial sites (B-site) in spinel structures, out of which 8 of tetrahedral (A-site) and 16 octahedral (B-site) sites are occupied by the metal cations[34]. Magnetic properties of ferrite nanoparticles depend on the strong exchange interaction between A and B ion sites in the crystal structure[35]. As an example, the magnetization of Cobalt ferrite nanoparticles which is due to the Co^{+2}cations distributed in B sites have been investigated by Shankar and coworkers. By substitution of Zn^{+2} cations, in tetrahedral sites of $CoFe_2O_4$, they have observed a decrease in magnetic moments and an increase in saturation magnetization. This result happens because the Zn^{+2} ions force Fe^{+3}ions to transform to Fe^{+2} to keep the neutrality of charge distribution in the structure[36,37].

Up to now, lack of an overall pattern to the behavior of ferrite MNPs has not been answered which can give scientists the freedom to find out the correct composition for their desired application without consuming time on the synthesis process with different compositions. In this paper, in the presence of citric acid, Cobalt, Nickel, and Zinc ion concentrations have been tuned to reduce the toxicity of MNPs and find a good pattern. There are different synthesis methods for ferrite MNPs such as auto-combustion synthesis, co-precipitation method[33,38–41], mechanical alloying[42], sol-gel[2,43], and so on. Each method has advantages over the other methods.

The hydrothermal method of synthesizing ferrite nanoparticles is controllable, yet highly parameter sensitive. Temperature and holding time are two main effective parameters that influence the microstructure and magnetic properties of these ferrites. Tengyan Wu et al. have studied these two parameters in 2019 on the synthetization process of Lanthanum substituted Zinc ferrites[44]. A significant result of their study is the increase in anisotropy constant, which is a key important parameter in our study, as the result of a corresponding increase in crystallite size with increasing temperature. There are a number of papers published in the application of this method to prepare nanoferrites for magnetic properties studies[9,27,44–47].

Here a combination of co-precipitation method and the hydrothermal process have been used to reach nanoparticles with good crystallinity in the presence of citric acid, not only to bind metal ions for forming a more stable structure but also to improve the biocompatibility of ferrite NPs. Although aware of the negative influence of an inert layer over MNPs on their high intensity magnetic properties, surface coating of various biocompatible nanomaterials such as citrate coated ferrite NPs is a strategy for surface chemical modifications that can improve the biocompatibility of nanoparticles[35].

Results and Discussion

Structural Characterization

Figure 1 shows Rietveld refined XRD diffractograms of Co–Ni-Zn-ferrite system with peaks corresponding to (220), (311), (400), (422), (511), (440) and (533) planes respectively, indexed to cubic spinel structure. In addition to these peaks, a low intense peak corresponding to (111) plane is observed. 2θ values calculated from prominent peaks are provided in Table S1. All peaks are consistent with the spinel ferrite phase

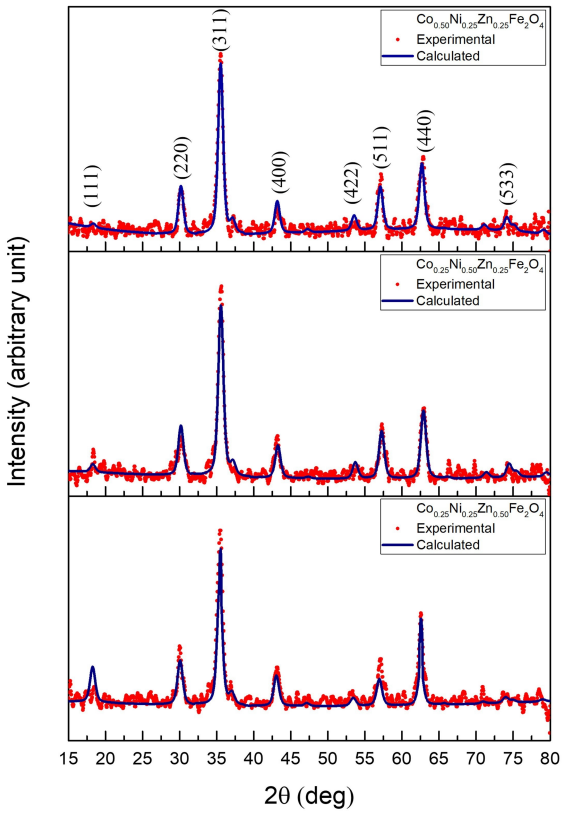

Figure 1. Room temperature X-ray diffraction data with Reitveld refined pattern of $Co_{0.50}Ni_{0.25}Zn_{0.25}Fe_2O_4$, $Co_{0.25}Ni_{0.50}Zn_{0.25}Fe_2O_4$ and $Co_{0.25}Ni_{0.25}Zn_{0.50}Fe_2O_4$ Ferrite nanoparticles.

according to JCPDS file no. 22–1086 ($CoFe_2O_4$), 74–2081 ($NiFe_2O_4$) and 82–1049 ($ZnFe_2O_4$) which confirm the composition of Co–Ni-Zn ferrite single crystalline phase. No observable secondary phases were found. Broad XRD patterns indicate that the ferrites are in nanometer size regime[48]. Rietveld refined structural data shown in Table 1 provides the crystallite sizes estimated to be ~ 8.76 *nm*, 8.35 *nm* and 7.05 *nm* and lattice parameters (a) ~ 8.39 Å, 8.34 Å and 8.40 Å for $Co_{0.50}Ni_{0.25}Zn_{0.25}Fe_2O_4$, $Co_{0.25}Ni_{0.50}Zn_{0.25}Fe_2O_4$ and $Co_{0.25}Ni_{0.25}Zn_{0.50}Fe_2O_4$ respectively. It can be seen that the lattice parameter decreases with increasing the nickel content from $Co_{0.50}Ni_{0.25}Zn_{0.25}Fe_2O_4$ to $Co_{0.25}Ni_{0.50}Zn_{0.25}Fe_2O_4$. Diffraction peaks got shifted toward the higher angle side with the increased substitution of Ni^{2+} ions as evidenced from Table S1. Since the ionic radius of Ni^{2+} ions (0.72 Å) is smaller than the ionic radius of Co^{2+} cations (0.74 Å), cobalt ion is substituted by nickel and thus the lattice parameter is decreased in accordance with Vegard's law [49] . As Co^{2+} and Ni^{2+} ions prefer to occupy in the octahedral sites, the decrement in lattice parameter can be attributed to the decrement in Co^{2+} cations present in octahedral site with the increase in Ni^{2+} concentration[50]. Later, the lattice parameter (a) seems to increase from 8.34 to 8.40 Å with the increase in zinc content from 0.25 to 0.50 suggesting the insertion of the zinc replacing nickel ion in the $Co_{0.25}Ni_{0.25}Zn_{0.50}Fe_2O_4$. In this case, diffraction peaks got shifted toward the lower angle side with the increased substitution of Zn^{2+} ions (evidenced from Table S2). Here higher occupancy of larger ionic radii Zn^{2+} (0.84 Å) cations replace smaller radii Ni^{2+} ions which will lead to an expansion of the structure and an increase in the lattice parameter to obey Vegard's law. It is expected that Zn^{2+} and half of the Fe^{3+} cations occupy the tetrahedral sites and the remaining Fe^{3+}, Co^{2+} and Ni^{2+} ions are distributed over the left octahedral sublattices constituting a partial inverse spinel crystal structure[51]. Therefore, the difference in behaviour of Ni and Zn substitution can be due to the difference in their ionic radii and ionic distribution at two sites[52,53].

Table 1. Crystallite size and lattice parameter (a) for the $Co_{1-(x+y)}Ni_xZn_yFe_2O_4$ (x, y = 0,0.25,0.5,0.75,1).

	Sample	Crystallite size (*nm*)
Figure 1	$Co_{0.50}Ni_{0.25}Zn_{0.25}Fe_2O_4$	8.76
	$Co_{0.25}Ni_{0.50}Zn_{0.25}Fe_2O_4$	8.35
	$Co_{0.25}Ni_{0.25}Zn_{0.50}Fe_2O_4$	7.05
Figure S1	$CoFe_2O_4$	9.53
	$Co_{0.75}Ni_{0.25}Fe_2O_4$	11.49
	$Co_{0.50}Ni_{0.50}Fe_2O_4$	14.46
	$Co_{0.25}Ni_{0.75}Fe_2O_4$	6.45
	$NiFe_2O_4$	7.26
Figure S2	$CoFe_2O_4$	9.53
	$Co_{0.75}Zn_{0.25}Fe_2O_4$	8.20
	$Co_{0.50}Zn_{0.50}Fe_2O_4$	7.62
	$Co_{0.25}Zn_{0.75}Fe_2O_4$	9.51
	$ZnFe_2O_4$	13.58
Figure S3	$NiFe_2O_4$	7.26
	$Ni_{0.75}Zn_{0.25}Fe_2O_4$	10.39
	$Ni_{0.50}Zn_{0.50}Fe_2O_4$	9.77
	$Ni_{0.25}Zn_{0.75}Fe_2O_4$	8.81
	$ZnFe_2O_4$	13.58

Fig. S1, S2 and S3 provide the XRD patterns of $Co_{1-x}Ni_xFe_2O_4$, $Co_{1-x}Zn_xFe_2O_4$, and $Ni_{1-x}Zn_xFe_2O_4$systems exhibiting the diffraction peaks of corresponding spinel ferrites. A similarly strong behavior favoring Vegard's law can be observed for the ferrite systems depicted in Fig. S1, S2 and S3. Figure 2 exhibits the lattice parameter changes with changing *x* concentration. Table 1 providing structural parameters given for Fig. S1, S2 and S3 clearly exhibits that the incorporation of Ni content decreases the lattice parameter whereas the incorporation of Zn content increases the lattice parameter which could be explained based on the ionic radii of Ni and Zn as explained above. The incorporation of Ni and Zn modifies the structural properties such as lattice parameter, ionic radii and ionic distribution at tetrahedral and octahedral sites of cubic spinel structure. The corresponding crystallite sizes and lattice parameters are tabulated in Table 1. All the crystallite sizes are found to be less than 15 nm and hence the nanoparticles are expected to be in superparamagnetic regime which is beneficial for magnetic hyperthermia. Crystallinity and lattice parameter indicate that all materials have crystallized into spinel-based ferrite system without any secondary phases.

Morphological observations

SEM and TEM analysis were carried out to observe the nanoparticles in powder form and when dispersed, respectively. The NPs in powder form were used for all XRD and VSM measurements. 15 different sample compositions were analyzed by EDX measurements, and all images were similar in terms of NP size and shape. Images in Figure 3 and Figure 4(a) show the images obtained for Sample 1 ($CoFe_2O_4$). Figure 4(a) shows a large cluster of NPs and the particles appear to be uniform in size and shape. In order to confirm the final composition of MNPs, EDX analysis was performed in different areas for each sample. Figure 4(b) shows the EDX analysis for these NPs. Table S2 includes final composition of each sample extracted from EDX analysis.

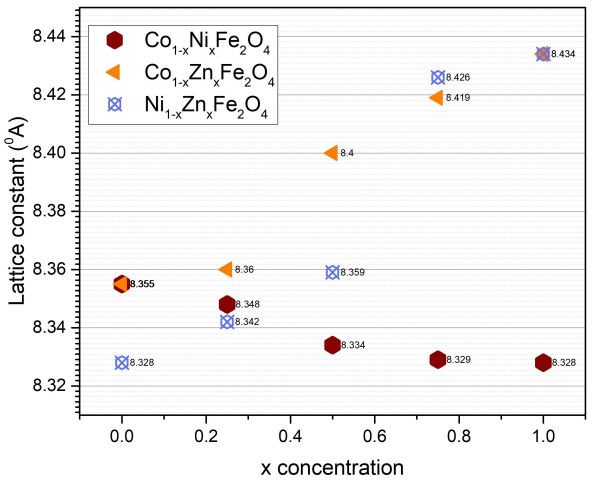

Figure 2. Lattice constant changes by changing the x concentration in $Co_{1-x}Ni_xFe_2O_4$, $Co_{1-x}Zn_xFe_2O_4$ and $Ni_{1-x}Zn_xFe_2O_4$ nanoparticles.

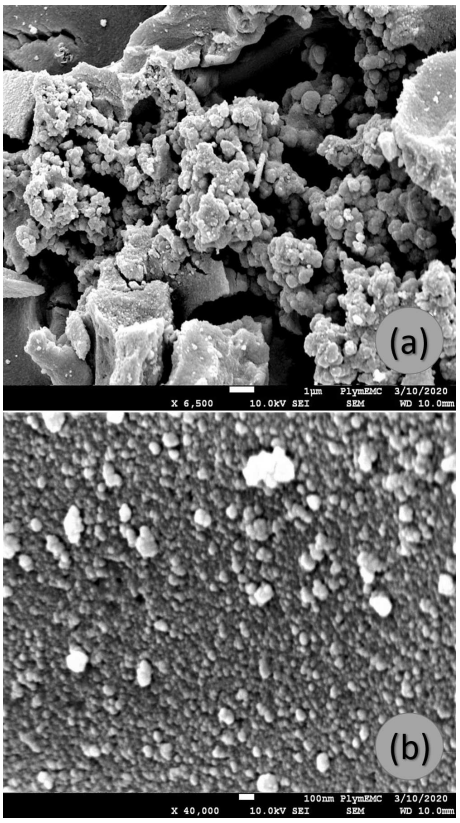

Figure 3. Morphological Characterization: (a) SEM of NPs at a magnification of 6,500 (scale bar: 1 μm), (b) SEM of NPs at a magnification of 40,000 (scale bar: 100 *nm*).

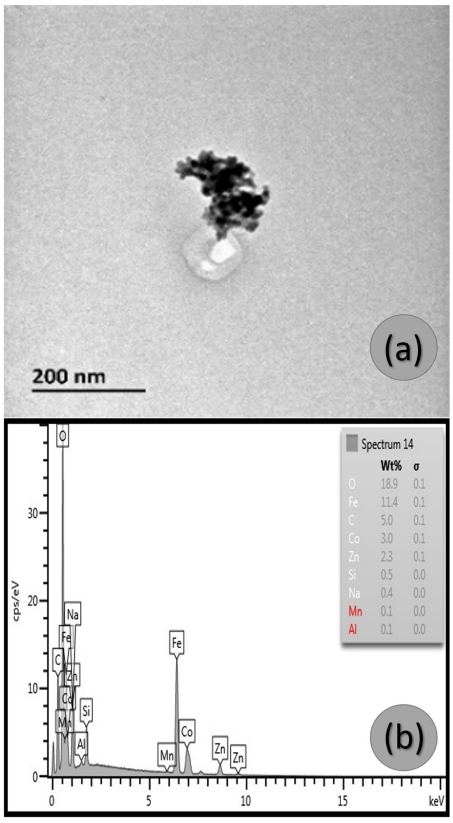

Figure 4. a) TEM of NPs showing particles to have sizes between 10 and 20 nm and (b) a sample EDX analysis of magnetic ferrite NPs.

Magnetic behaviour

Using VSM analysis, the remanence, saturation and coercivity of $Co_{1-(x+y)}Ni_xZn_yFe_2O_4$ ferrite samples were measured. Table S2 and figures S4 to S7 in the supplementary letter, show the extracted data from EDX analysis, magnetic hysteresis loops and their characteristic features of all 15 samples. While the important graph representations of these data can be seen in Figure 5 and Figure 9.

Sample numbers are indicated as follows: (S1): $CoFe_2O_4$, (S2): $Co_{0.75}Ni_{0.25}Fe_2O_4$, (S3): $Co_{0.75}Zn_{0.25}Fe_2O_4$, (S4): $Co_{0.50}Ni_{0.50}Fe_2O_4$, (S5): $Co_{0.50}Ni_{0.25}Zn_{0.25}Fe_2O_4$, (S6): $Co_{0.50}Zn_{0.50}Fe_2O_4$, (S7): $Co_{0.25}Ni_{0.75}Fe_2O_4$, (S8): $Co_{0.25}Ni_{0.50}Zn_{0.25}Fe_2O_4$, (S9): $Co_{0.25}Ni_{0.25}Zn_{0.50}Fe_2O_4$, (S10): $Co_{0.25}Zn_{0.75}Fe_2O_4$, (S11): $NiFe_2O_4$, (S12): $Ni_{0.75}Zn_{0.25}Fe_2O_4$, (S13): $Ni_{0.50}Zn_{0.50}Fe_2O_4$, (S14): $Ni_{0.25}Zn_{0.75}Fe_2O_4$ and (S15): $ZnFe_2O_4$.

The counterplots of the hysteresis loops is employed to discuss the changes in the magnetic behavior of these samples. Since the loops indicate symmetrical behaviour, which is a typical of AC-magnetometery [54], then the data measured from -15 *kOe* to $+15$ *KOe* (which is half of a complete loop) is used.

First, Co/Ni ferrite powders with an average size of $10-13$ *nm*, have been studied via vibrating sample magnetometer (VSM). As demonstrated in Figure 5, and Table S2, by increasing the Ni^{+2} substituted ion content of the FCC ferrite structure, an obvious decrement in remanent magnetization (the magnetization value at $H=0$) is occurred. The light green area also indicates the minimum amount of magnetization which includes the coercive field area. It is clear that by increasing the *Ni* content, this area becomes narrower than high *Co* content ferrite powders which indicates the transform from hard to soft magnetic nanoparticles.

Secondly,*CoZn* samples were prepared. Unfortunately, the sample with 0.25 substitution of *Zn* had to be substituted with about 0.40 *Zn* (obtained from EDX results). As the area which could be covered by this sample was being expected to have magnetization values in a range of 17 to 34 emu/g, it can still be seen the overall trace and behavior of magnetic properties. By increasing the Zn^{+2} substituted ion content of the FCC ferrite structure, it is possible to produce the materials with the lowest magnetization and coercivity values up to 6 *Oe* which is really small in value and indicates the superparamagnetic behavior, see Figure 7.

Now let's assume simultaneous substitution of *Ni* and *Zn* ions with 4 different ratios with fixed amount of *Co* (0.25) in the structure. As depicted in Figure 8(a) and (b), the magnetization and saturation magnetization curves initially, appear to be a little random. This behaviour results from a synergic entanglement of two main parameters; the crystallite size and composition of the Ferrite powder. The first one is well

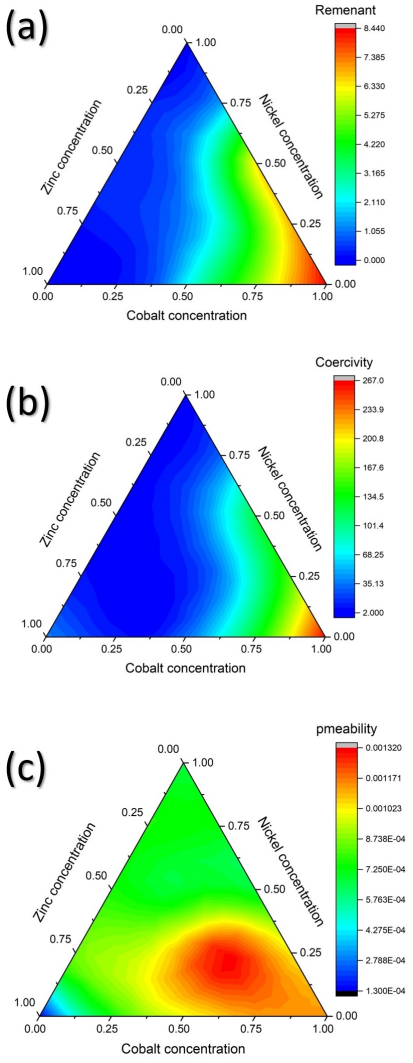

Figure 5. Diagram of Magnetic properties: (a) Compositional dependance of Coercive field, (b) Compositional dependance of Remanent and (c) Compositional dependance of incremental permeability.

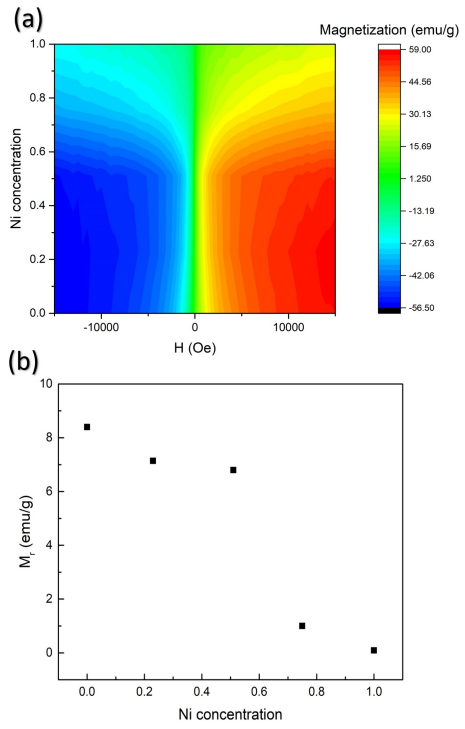

Figure 6. Magnetic response and (b) Remanent magnetisation of Co ferrite with different substituted percentages of Ni ions in the structure by applying magnetic fields in range of 15kOe to −15kOe

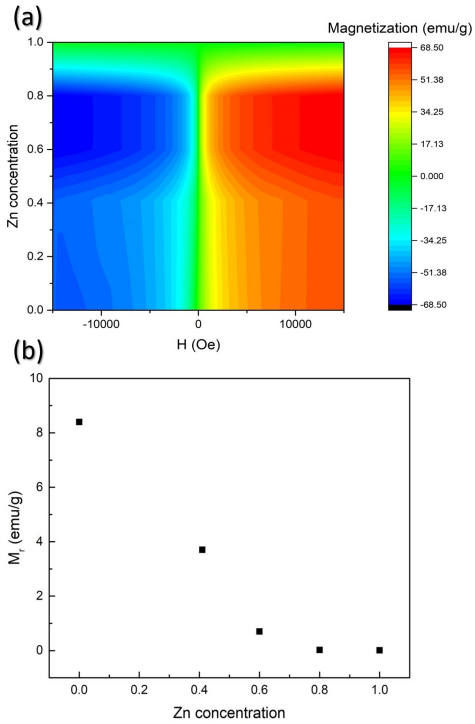

Figure 7. Magnetic response and (b) Remanent magnetisation of Co ferrite with different substituted percentages of Zn ions in the structure by applying magnetic fields in range of 15kOe to −15kOe.

explained in ref.[27,44] while the ferrite composition is the focus of our paper. An increase of crystallite size leads to decrease in spin disordering and thus an increase in the saturation magnetization value.

it is clearly seen that for the samples with no Nickel or Zinc ions, i.e. Binary ferrites, they have almost low and predictable amounts of magnetization values but for the middle area which is related to triple ion ferrites, $Co_{0.23}Ni_{0.25}Zn_{0.52}Fe_2O_4$and $Co_{0.23}Ni_{0.47}Zn_{0.30}Fe_2O_4$, it can be seen that the higher values and surprisingly the highest value is related to the higher ratio of Zinc rather than Nickel. This shows that by using the proper amount of ions in the structure not only the magnetic properties can be managed but also one can have the advantage of synergistic behavior of these ions.

Magnetic permeability is calculated by the slope of the B–H curve which is proportional to the M–H curve and is a measure of the material's response to an applied magnetic field. In a nonlinear medium, the permeability may depend on the

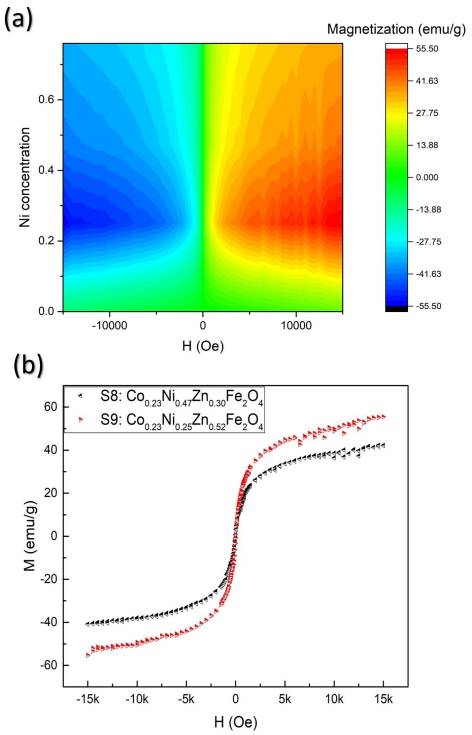

Figure 8. Magnetic response of $Co_{0.25}Ni_xZn_{0.75-x}Fe_2O_4$ ferrite with different substituted percentages of Zn and Ni ions in the structure by applying magnetic fields in range of 15kOe to −15kOe and (b) Magnetic hysteresis loops of selected samples.

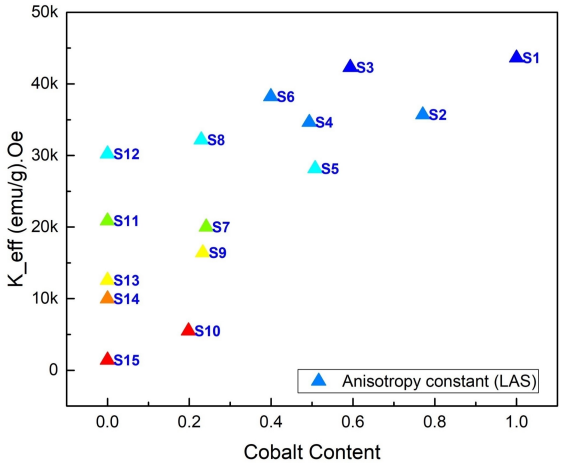

Figure 9. Effective anisotropy constant of different samples by using LAS method.

strength of the magnetic field. The slope of the B–H curve is its incremental permeability at a given point. However, sometimes the permeability is measured from the origin to the location of interest, and that slope is called its apparent permeability, μ. For non-magnetic materials that do not saturate, the curve has a fixed slope approximately equal to μ_0. While, for magnetic materials it is useful to study the magnetic incremental permeability (MIP) which is defined as follows:

$$\Delta B \propto \mu_\Delta \Delta H \tag{1}$$

and is an important parameter to evaluate the physical/mechanical properties, which are correlated with the magnetic properties of the material[55–60]. From this point of view, the change in magnetic properties may be as a result of microstructural changes which directly affect the mechanical properties of the material[59,61].

In Figure 5(c) the incremental permeability is being well calculated for the applied H of 5 *kOe* to 15 *kOe*. The incremental permeability of the Zinc ferrite MNPs, has the lowest value as expected. The presence of the Zn^{+2} cations as a nonmagnetic material highly decreases the magnetization values which will be well increased by substitution of Co^{+2} cations in the structure. The same behavior happens for substitution of Ni^{+2} ions but the increase in magnetization values for the same increase in an applied magnetic field is not as sensitive as in the Cobalt case. Aside from this increasing pattern that can be seen in two parameter changes of the ions, it is really interesting that with lower amounts of Co^{+2} cations in the structure, only by finding the correct values of x and y in the $Co_{1-(x+y)}Ni_xZn_yFe_2O_4$, the highest value for MIP is obtained. In this study, the highest value belongs to $Co_{0.51}Ni_{0.26}Zn_{0.23}Fe_2O_4$, which might be of a great importance in biomedical applications as one could reach to the maximum permeability and magnetization by using a Zn^{+2} ions as the less toxic precursor in comparison with Ni^{+2} and Co^{+2}.

As discussed in the introduction section, the anisotropy constant of a material can be a measure of its potential for hyperthermia treatment applications. The law of approach to saturation (LAS) is a reliable method to determine the anisotropy constant value. The dependence of magnetization (M) on the applied magnetic field (H) near the saturation magnetization M_s region is the advantage of this method. The corresponding equation can be written as

$$M = M_s\left(1 - \frac{a}{H} - \frac{b}{H^2} - \ldots\right) \tag{2}$$

Thus

$$\frac{dM}{dH} = M_s\left(\frac{a}{H^2} + \frac{2b}{H^3} - \ldots\right) \tag{3}$$

Where

$$b = \frac{\beta K_{eff}^{\ 2}}{M^2} \tag{4}$$

β is a constant parameter in Equation 4 which its value for uniaxial anisotropy is $\frac{4}{15}$.

The anisotropy constant measured here is in agreement with published data using the LAS method at higher magnetic fields[62–65].

As it can be seen in Figure 9, pure Cobalt ferrite nanoparticles have the highest anisotropy constant which obviously

decreases with decreasing the Cobalt ion contribution in the structure. But this reduction is highly affected by substituted ions. In a competition between Zinc and Nickel ions, in case of pure Nickel ferrite nanoparticles (S11) and pure Zinc ferrite nanoparticles (S15), Zinc MNPs will exhibit the minimum anisotropy constant. Hence we may conclude that Zinc ion substitution is going to have a more negative effect than Nickel ions. But being more precise, samples $NiFe_2O_4$ (S11) vs $Ni_{0.75}Zn_{0.25}Fe_2O_4$ (S12) and $Co_{0.25}Ni_{0.75}Fe_2O_4$ (S7) vs $Co_{0.25}Ni_{0.50}Zn_{0.25}Fe_2O_4$ (S8) are evidence of its positive effect in multi-ion substitutions. These results highly recommend further investigations by researchers on these types of structures to get the best hyperthermia efficiency by using less injection of the magnetic materials to reduce lateral side effects of this treatment.

Conclusion

$Co_{1-(x+y)}Ni_xZn_yFe_2O_4$ magnetic nanoparticles with uniform size and cubic structure for possible magnetic fluid hyperthermia (MFH) applications have been successfully synthesized. By changing the composition, it is possible to tune the magnetic properties, especially the anisotropy constant, K_{eff}, which is being calculated using the LAS method. From the magnetic point of view, ferrite MNPs with the chemical formula of $Co_{1-(x+y)}Ni_xZn_yFe_2O_4$ as ternary ferrite nanoparticles have the ability to reach higher anisotropy constants and hence heating efficiency by finding the optimal composition rather than using pure nickel or pure zinc ferrite nanoparticles.

This success in customizing magnetic properties to reach higher magnetic properties by using non-magnetic/ less toxic materials might be another good starting point for researchers to focus more on their possible applications.

Supporting Information Summary

The supporting information file includes; Synthesis and characterization details of ferrite nanoparticles having chemical composition $Co_{1-(x+y)}Ni_xZn_yFe_2O_4$, where $x, y = 0.00, 0.25, 0.50, 0.75, 1.00$, tables and figures which have been addressed in the main text for EDX, XRD and VSM characterizations.

Acknowledgements

We would like to thank Mr. Alireza Nikzad for his expert advice in the lab.

Conflict of Interest

The authors declare no conflict of interest.

Keywords: Anisotropy constant · Ferrite · Heat Efficiency · Hydrothermal synthesis · Magnetic Properties

[1] K. L. Routray, B. Behera, *Mater. Elektron.* **2018**, *29*, 14248–14260.
[2] V. K. Mande, D. N. Bhoyar, S. K. Vyawahare, K. M. Jadhav, *Mater. Elektron.* **2018**, *29*, 15259–15270.
[3] C. C. Berry, *J. Phys. D* **2009**, *42*, 22403- 22412.
[4] S. Arunima Rajan, M. Sharma, N. Kumar Sahu, *J. Supercond. Novel Magn.* **2020**, *33*, 1603–1609.
[5] A. Farzin, S. Hassan, R. Emadi, S. A. Etesami, J. Ai, *Mater. Sci. Eng.* **2019**, *98*, 930–938.
[6] S. Y. Srinivasan, K. M. Paknikar, D. Bodas, V. Gajbhiye, *Nanomedicine* **2018**, *13*, 1221–1238.
[7] S. Mohapatra, S. Rout, S. Maiti, T. Maiti, A. Panda, *J. Mater. Chem.* **2011**, *21*, 9184–9193.
[8] M. Colombo, S. Carregal-Romero, M. F. Casula, L. Gutiérrez, M. P. Morales, I. B. Böhm, J. T. Heverhagen, D. Prosperi, W. J. Parak, *Chem. Soc. Rev.* **2012**, *41*, 4306–4334.
[9] A. S. Ahmed, R. V. Ramanujan, *Sci. Rep.* **2015**, *5*, 13773- 13783.
[10] S. R. Gibin, P. Sivagurunathan, **2017**, *28*, 1985–1996.
[11] S. Sumathi, V. Lakshmipriya, **2017**, *28*, 2795–2802.
[12] Q. A. Pankhurst, J. Connolly, S. K. Jones, J. Dobson, *J. Phys. D* **2003**, *36*, R167- R181.
[13] K. Maier-Hauff, F. Ulrich, D. Nestler, H. Niehoff, P. Wust, B. Thiesen, H. Orawa, V. Budach, A. Jordan, *J. Neuro-Oncol.* **2011**, *103*, 317–324.
[14] A. Jordan, A. Scholz, R. Wust, P. Fähling, H. Felix, *J. Supercond. Novel Magn.* **1999**, *201*, 413–419.
[15] J. P. Fortin, C. Wilhelm, J. Servais, C. Ménager, J. C. Bacri, F. Gazeau, *J. Am. Chem. Soc.*, **2007**, *129*, 2628–2635.
[16] C. P. Gooneratne, A. Kurnicki, S. Yamada, S. C. Mukhopadhyay, J. Kosel, *PLoS One* **2013**, *8*, 1-14.
[17] M. Johannsen, B. Thiesen, P. Wust, A. Jordan, *Int. J. Hyperthermia* **2010**, *26*, 790–795.
[18] H. Mamiya, Y. Takeda, T. Naka, N. Kawazoe, G. Chen, B. Jeyadevan, *J. Nanomater.* **2017**,*1*, 1–7.
[19] W. J. Atkinson, I. A. Brezovich, D. P. Chakraborty, *IEEE Trans. Biomed. Eng.* **1984**, *BME-31*, 70–75.
[20] A. Jordan, *Int. J. Hyperthermia* **2009**, *25*, 512–516.
[21] Naiyin Zhang, *Magnetic Nanocomposites, Fields for Tissue Engineering Applications*, ProQuest Dissertations Publishing, University of California, Riverside, **2017**, *p. 24.*
[22] R. E. Rosensweig, *J. Supercond. Novel Magn.* **2002**, 370–374.
[23] E. Fantechi, C. Innocenti, M. Albino, E. Lottini, C. Sangregorio, *J. Supercond. Novel Magn.* **2015**, *380*, 365–371.
[24] G. D. Hogan, W. E. Rauser, *New Phytol.* **1979**, *83*, 665–670.
[25] L. Horev-Azaria, G. Baldi, D. Beno, D. Bonacchi, U. Golla-Schindler, J. C. Kirkpatrick, S. Kolle, R. Landsiedel, O. Maimon, P. N. Marche, J. Ponti, R. Romano, F. Rossi, D. Sommer, C. Uboldi, R. E. Unger, C. Villiers, R. Korenstein, *Part. Fibre Toxicol.* **2013**, *10*, 1-17.
[26] R. S. de Biasi, L. H. G. Cardoso, *Phys. B*, **2012**, *407*, 3893–3896.
[27] F. Ding, J. Lin, T. Wu, H. Zhong, *Appl. Phys. A* **2020**, *126*, 2211-2219.
[28] G. Vaidyanathan, S. Sendhilnathan, R. Arulmurugan, *J. Supercond. Novel Magn.* **2007**, *313*, 293–299.
[29] M. Ul Islam, M. Uddin Rana, T. Abbas, *Mater. Chem. Phys.* **1998**, *57*, 190–193.
[30] R. Arulmurugan, B. Jeyadevan, G. Vaidyanathan, S. Sendhilnathan, *J. Supercond. Novel Magn.*, **2005**, *288*, 470–477.
[31] M. S. Tomar, S. P. Singh, O. Perales-Perez, R. P. Guzman, E. Calderon, C. Rinaldi-Ramos, *Microelectron. J.* **2005**, *36*, 475–479.
[32] P. Wang, Y. Li, Y. Jing, Z. Xu, X. Tang, *Mater. Elektron.* **2019**, *30*, 21004–21010.
[33] G. Sathishkumar, C. Venkataraju, K. Sivakumar, *Mater. Elektron.*, **2011**, *22*, 1715–1724.
[34] B. D. Cullity, C. D. Graham, *Introduction to Magnetic Materials, 2nd Edition, Wiley. A John Wiley & sons*, **2015**, p. 568.
[35] M. Mohamed, M. Yehia, *J. Alloys Compd.* **2014**, *615*, 181–187.
[36] G. D. Dwivedi, K. F. Tseng, C. L. Chan, P. Shahi, J. Lourembam, B. Chatterjee, A. K. Ghosh, H. D. Yang, S. Chatterjee, *Phys. Rev. B* **2010**, *82*, 44281-44285.
[37] B. Prajapati, S. Kumar, A. Ghosh, O. Thakur, *Mater. Elektron.* **2016**, *27*, 13259–13265.
[38] P. Sivagurunathan, S. R. Gibin, *Mater. Electron.* **2016**, *27*, 2601–2607.
[39] P. Sivagurunathan, S. R. Gibin, *Mater. Elektron.* **2016**, *27*, 8891–8898.
[40] K. Hedayati, Z. Behesht-Ara, D. Ghanbari, *Mater. Elektron.*, **2017**, *28*, 1–9.

[41] S. Mirzaee, Y. Azizian-Kalandaragh, P. Rahimzadeh, *Solid State Sci.* **2020**, *99*, 1060521- 1060529.
[42] C. Behera, R. N. P. Choudhary, P. R. Das, *Mater. Elektron.* **2015**, *26*, 2343–2356.
[43] P. M. M. Gazzali, G. Chandrasekaran, *Mater. Elektron.* **2014**, *25*, 702–709.
[44] T. Wu, D. Li, M. Wei, H. Han, *Appl. Phys. A* **2019**, *125*, 2431-2438.
[45] T. Wu, F. Ding, D. Li, H. Zhong, *ChemistrySelect* **2020**, *5*, 14978–14985.
[46] T. Wu, G. Shen, F. Ding, D. Li, H. Zhong, *Mater. Chem. Phys.*, **2020**, *252*, 1233281-1233288.
[47] S. U. Haque, K. K. Saikia, G. Murugesan, S. Kalainathan, *J. Alloys Compd.* **2017**, *701*, 612–618.
[48] C. E. Krill, R. Birringer, *Philos. Mag. A* **2009**, *77*, 621–640.
[49] N. B. Velhal, N. D. Patil, A. R. Shelke, N. G. Deshpande, V. R. Puri, *AIP Adv.* **2015**, *5*, 0971661-09716611.
[50] G. Sathishkumar, C. Venkataraju, K. Sivakumar, *Mater. Sci. Appl.* **2010**, *1*, 19–24.
[51] F. S. M. Sinfro nio, S. Sinfro nio, P. Y. C. Santana, S. F. N. Coelho, F. C. Silva, A. S. de Menezes, S. K. Sharma, *J. Electron. Mater.* **2017**, *46*, 1145–1154.
[52] C. Srinivas, B. V. Tirupanyam, A. Satish, V. Seshubai, D. L. Sastry, O. F. Caltun, *J. Supercond. Novel Magn.* **2015**, *382*, 15–19.
[53] M. ben Ali, K. el Maalam, H. el Moussaoui, O. Mounkachi, M. Hamedoun, R. Masrour, E. K. Hlil, A. Benyoussef, *J. Supercond. Novel Magn.* **2016**, *398*, 20–25.
[54] Y. F. Ponomarev, *Phys. Met. Metallogr.* **2008**, *105*, 263–274.
[55] H. E. Chen, S. Xie, H. Zhou, Z. Chen, T. Uchimoto, T. Takagi, Y. Kensuke, *Int. J. Appl. Electromagn. Mech.* **2014**, *45*, 379–386.
[56] W. S. Cho, T. S. Yoon, H. Lee, C. O. Kim, *J. Supercond. Novel Magn.* **2000**, *215*, 680–683.
[57] W. S. Cho, H. Lee, C. O. Kim, *Thin Solid Films* **2000**, *375*, 51–54.
[58] W. S. Cho, H. B. Lee, T. S. Yoon, Y. W. Lee, J. H. Kim, C. O. Kim, *J. Supercond. Novel Magn.* **2002**, *239*, 304–306.
[59] B. Gupta, T. Uchimoto, B. Ducharne, G. Sebald, T. Miyazaki, T. Takagi, *NDT&E Int.* **2019**, *104*, 42–50.
[60] G. Piao, J. Guo, T. Hu, Y. Deng, H. Leung, *Sens. Actuators A* **2019**, *295*, 244–258.
[61] V. T. Zaspalis, V. Tsakaloudi, M. Kolenbrander, *J. Supercond. Novel Magn.* **2007**, *313*, 29–36.
[62] L. Kumar, M. Kar, *J. Supercond. Novel Magn.* **2011**, *323*, 2042–2048.
[63] F. L. A. Machado, J. M. Soares, O. L. A. Conceição, E. S. Choi, L. Balicas, *J. Supercond. Novel Magn.* **2017**, *424*, 323–326.
[64] S. Mirzaee, S. Mahdavifar, S. F. Shayesteh, *J. Supercond. Novel Magn.* **2018**, *31*, 217–223.
[65] J. Herbst, F. Pinkerton, *Phys. Rev. B: Condens. Matter Mater. Phys.* **1998**, *57*,10733.

Submitted: November 27, 2020
Accepted: January 10, 2021